Compensation Alternatives for Power Sharing Errors in Multi-Port Converters for Hybrid DC/AC Microgrids

Geber Villa, Sarah Saeed, Pablo García, Carlos Gómez-Aleixandre and Ramy Georgious
Dept. of Electrical, Electronic, Computers and Systems Engineering
University of Oviedo
Gijón, 33204, Spain
villageber@uniovi.es, saeedsarah@uniovi.es, garciafpablo@uniovi.es,
gomeztcarlos@uniovi.es, georgiousramy@uniovi.es

***Abstract*—This paper proposes several alternatives for the compensation of power sharing errors in the DC bus of hybrid DC/AC microgrids. The case of study consists in a multi-port converter used for the interconnection of a AC grid-tied converter, a battery, a supercapacitor and a regenerative DC load that has to be supplied. The storage elements and the load are connected by means of DC/DC converters. The power sharing between the battery and the supercapacitor is determined by using an estimation of the load power. However, due to errors in sensors or control actions of the converters, the real load power is not exactly equal to the estimated one and hence a power mismatch is produced. Those mismatches are absorbed by the DC-link voltage, which is controlled by the grid-tied converter. However, considering restrictions in the grid-tied converter, the differences in the power sharing can compromise the operation and the stability of the system. In this paper, three compensation methods are proposed and compared. The proposed methods allow for the stable operation of the system, even with noticeable errors in the power sharing.**

I. Introduction

Local small-scale power systems are being developed to promote the introduction of renewable energies, since they are closely related to distributed generation unlike the conventional ones. The concept of microgrid appears in order to categorize this type of systems, which are evolving over time [1]. Microgrids usually have some energy storage units to support the renewable power generation, which is nondeterministic. Different kind of energy storage systems can be installed, some of them being more dedicated to the energy needs (batteries), while others show their advantages in terms of power capability (supercapacitors) [2], [3]. In order to exploit the advantages of the different types of energy storage system, microgrids can use an hybrid implementation (e.g. battery and supercapacitor), so that a flexible and reliable operation is achieved [4], [5].

Batteries have relatively high energy density but they are not suitable when suffering high variations of power. This is because the internal electrochemical reactions inside the battery produce a process of degradation [6]. To face this problem, supplementary supercapacitors can be used since they work properly under high variations of power [7]–[9], though they have low energy density. Therefore, it is necessary to perform a power sharing between battery and supercapacitor [10], [11], so that the battery manages the main power exchanges (energy source) whereas the supercapacitor is in charge of the transient power variations (power source) [12]–[15].

However, any error in the calculation of the power sharing produces a mismatch, which may disturb the performance of the system. Errors in the sensors, in the estimation of the power load or in the control actions of the converters often appear during the operation of a power system. Thus, the influence of these mismatches should be analyzed in order to determine the resultant effects, which might affect the integrity of the system.

The analyzed case is a hybrid DC/AC microgrid which is composed of a DC load, a battery and a supercapacitor. The electrical diagram, which is based on the use of intelligent Power Electronics Building Blocks (iPEBB) [16], is shown in Fig. 1. An extra capacitor is connected to the DC grid to create a DC bus with an established DC voltage. Additionally, an inverter is connected to exchange energy with the AC grid. The objective of this paper is to analyze the power mismatches problem in the DC/AC microgrid and to propose several compensation alternatives.

This paper is organized as follows. In Section II, an explanation of the problems that can arise when power sharing is applied to the DC/AC microgrid is addressed. In Section III, an analysis of the different compensation techniques suited for mitigating the different issues is discussed. In Section IV and Section V, simulation and experimental results are obtained in order to validate the proposed system. Finally, in Section VI, conclusions about the accomplished work are discussed.

The present work has been partially supported by the predoctoral grants program FPU for the formation in university teaching of Spain MECD under the grant IDs FPU16/06829 and FPU16/05313. This work also was supported in part by the Research, Technological Development and Innovation Program Oriented to the Society Challenges of the Spanish Ministry of Economy and Competitiveness under grant ENE2016-77919-R; by the European Union through ERFD Structural Funds (FEDER); and by the government of Principality of Asturias, under IDEPA grant 2017 Thyssen SV-PA-17-RIS3-3.

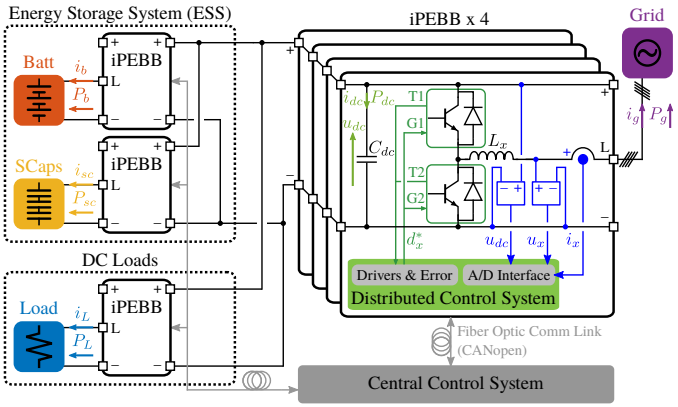

Fig. 1. Electrical diagram of the hybrid DC/AC microgrid based on the use of intelligent Power Electronics Building Blocks (iPEBB).

II. Power Sharing Issues

The simplified DC/AC microgrid is made up of several power units interconnected by a multi-port power converter through a capacitor which creates a DC bus. The considered units are an aggregated regenerative DC load, which represents the different loads connected to the DC grid; a Li-ion battery; a supercapacitor, and a grid-tied interlinking converter connected to the AC grid (Fig. 1). In order to supply the DC load, a power sharing between the different devices of the system is done. The base load demand is provided by the AC grid, whereas the peak load demand is provided by the energy storage system (ESS): low frequency components are supplied by the battery (energy source) whereas the high frequency components are supplied by the supercapacitor (power source). By using two low-pass/high-pass filters with different cutoff frequencies, it is possible to tweak the power sharing as desired.

Fig. 2 shows the proposed control diagram to carry out the power sharing mechanism. The power sharing is computed by the central controller, which sent the initial power references (P^*_{x0}) to the current control of the different distributed control units, in order to manage the power of the different devices in the system. Still, it requires to have an accurate measurement of the power by each of the converter units. However, accuracy of the sensors or saturation phenomena in the control action of any unit will induce differences in the real power sharing.

Focusing on the DC side of the system, the power balance expression which links the different power units (load: P_L, battery: P_b, supercapacitor: P_{sc}, grid: P_g and DC bus capacitor: P_{dc}) is given by (1).

$$P_L + P_b + P_{sc} + P_g + P_{dc} = 0 \tag{1}$$

When a power mismatch occurs, (1) is not longer equal to zero. In that case, the power surplus or shortage has to be delivered/absorbed by some power units to compensate for the difference. In the present application, the DC-link capacitor acts as the buffer for it and hence the power mismatches produces a variation in the DC-link voltage. Considering the grid-tied DC/AC inverter is controlling the DC-link voltage, the variation will depend on the stiffness of that control. The

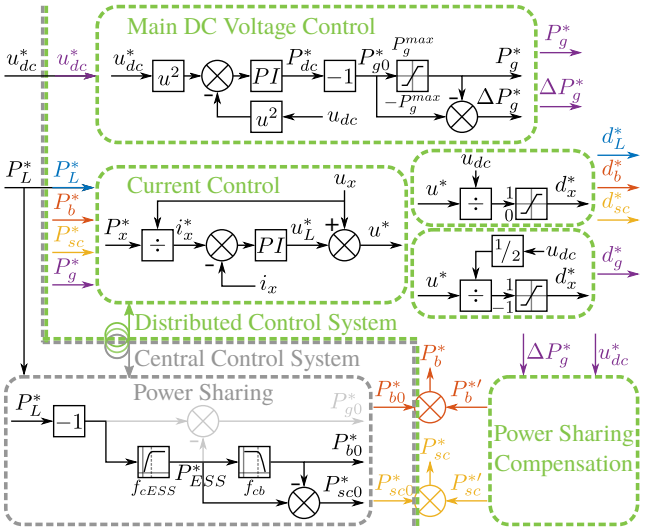

Fig. 2. Control diagram of the hybrid DC/AC microgrid. Gray units are integrated in the central control system whereas green units are integrated in the distributed control units.

variations induced in the DC-link voltage because of the power mismatch are also affected by the maximum power that can be managed by the grid DC/AC converter, since the converter can reach saturation and therefore not be able to provide the required power to maintain the DC-link voltage at an appropriate level.

Fig. 3 shows the power sharing issues which appear when the grid power is limited, so that saturation in the grid DC-link voltage controller is produced. When the grid power reaches the minimum/maximum limit, the DC-link voltage either drops to the rectifier level or rises to fault values. This way, the system operation is compromised and correction actions are required to take back DC voltages within safe values.

In order to solve this problem, it is necessary to dynamically correct power mismatches to ensure a suitable operation. Considering that power mismatches are normally a transient problem, often with fast dynamics, this paper proposes several alternative compensation methods relaying on a modified operation of the ESS.

A new control module is introduced into the control diagram (Fig. 2) with a view to performing the power sharing compensation. Extra power references ($P^{*\prime}_x$) are computed by this module and commanded together with the initial power references (P^*_{x0}) to the current control loop. Since it is required to compensate the power mismatches rapidly, the power sharing compensation is internally performed by each distributed control unit.

III. Compensation Techniques

As mentioned above, power mismatches in the power sharing produce a deviation of the DC bus voltage from the nominal value. Thus, some kind of correction has to be applied to mitigate the problem. Three different compensation techniques are proposed: 1) open loop power reference compensation,

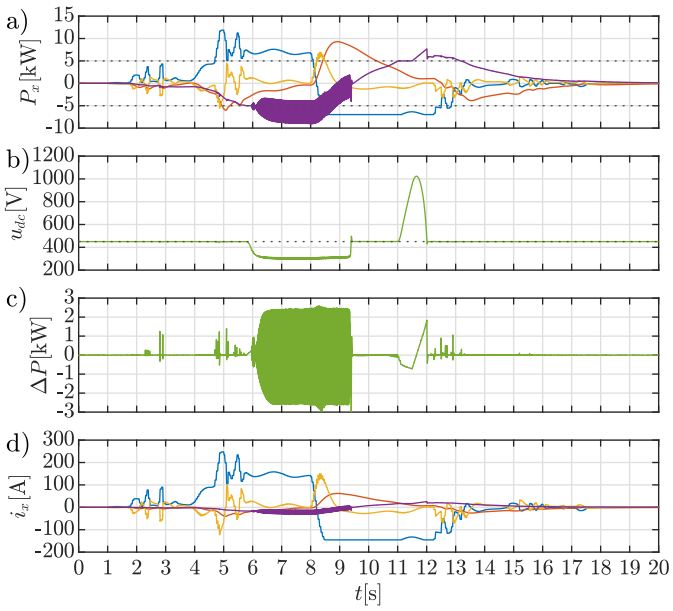

Fig. 3. Power sharing issues when the grid power is limited (−5 to 5 kW). a) Power consumption; b) DC-link voltage; c) Power mismatch; d) Current comsumption. Color legend: blue, load; red, battery; orange, supercapacitor; purple, grid; green, DC bus.

2) auxiliary DC voltage control and 3) closed loop power reference compensation.

The big challenge is to estimate properly the power mismatch. It would be necessary to measure the power of every unit which comprise the whole system, but this would require the installation of an extra current sensor for the load (the power generation units are already controlled so they need a current sensor) and the cost would increase. Moreover, errors in the calibration of the sensors will produce additional power mismatches since the measurements of the different variables will not be completely accurate.

Alternatively, an estimation method for the compensation power can be done by analyzing the shape of the grid DC-link voltage controller. The main (grid) DC voltage control is controlled by the grid-tied converter using a quadratic voltage control (QVC) [17] as shown in Fig. 2, so that the control action is expressed in terms of power. If saturation in the grid-tied converter is produced, the controller will not longer be able to apply the required power. The remaining power (ΔP_g^*) can be considered as the power mismatch and, under the presented control structure, is assigned to the grid-tied converter.

A. Open loop power reference compensation

The first compensation technique consists of tracking the power mismatch and trying to introduce into the system the opposite power.

The power mismatch has to be provided by the ESS since the grid-tied converter is working under saturation conditions. Since the supercapacitor is the device in charge of managing fast power variations and the battery is responsible for giving/absorbing energy, a low-pass filter is used to determine the extra references of both devices ($P_b^{*\prime}$ and $P_{sc}^{*\prime}$), using the power mismatch as an input, as shown in Fig. 4.

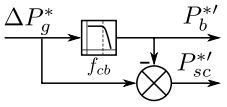

Fig. 4. Open loop power sharing compensation.

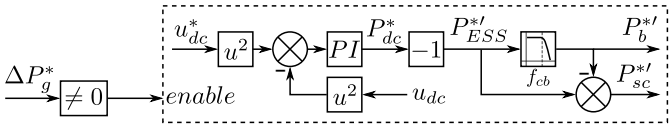

Fig. 5. Auxiliary DC voltage control.

This way, the power mismatch is mitigated and hence the DC bus voltage deviation is reduced, so that the system is kept in safe conditions.

B. Auxiliary DC voltage control

The second compensation technique consists of implementing an auxiliary DC voltage control in the ESS to support the main (grid) DC voltage control during saturation events. The proposed scheme is shown in Fig. 5. Under normal conditions, only the main DC voltage control has to be active. Therefore, it is necessary to determine the enabling strategy which triggers the auxiliary DC voltage control.

The enabling strategy is similar to the one applied for the open loop power reference compensation. When saturation is produced in the main DC voltage control, there is a power mismatch which needs to be corrected. Thus, the auxiliary DC voltage control can be enabled when saturation is detected (grid power mismatch is not zero).

The resultant control action of the auxiliar DC voltage control is the extra ESS power reference ($P_{ESS}^{*\prime}$), so a low-pass filter is used to determine the extra reference of the battery ($P_b^{*\prime}$) and the extra reference of the supercapacitor ($P_{sc}^{*\prime}$).

Two different implementations of the controller will be studied for this compensation technique: pure P controller and PI controller. The reasoning behind analyzing both controllers is that the auxilary DC voltage control is only enabled from time to time. Therefore, an integral action can be clampled to a non-zero value whenever the control is disabled, so that the performance of the PI controller could be affected.

C. Closed loop power reference compensation

Analyzing in detail the main DC voltage control, which is shown in Fig. 2, it can be observed that the grid power reference mismatch (ΔP_g^*) corresponds to the error between the desired grid power reference and the applied one.

Therefore, it is possible to implement a closed loop power reference compensation by managing this error through a PI controller, as shown in Fig. 6. This way, it is expected to improve the results obtained from the open loop power reference compensation if the controller is tuned properly.

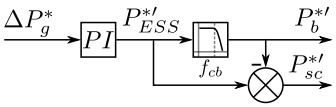

Fig. 6. Closed loop power sharing compensation.

TABLE I
SYSTEM PARAMETERS.

Parameter	Value
Filter inductor inductance (L)	1.7 mH
Filter inductor resistance (R)	0.33 Ω
DC-link total capacitance (C_{dc})	750 μF
Nominal DC-link voltage	450 V
Nominal grid line RMS voltage	245 V
Nominal grid frequency	50 Hz
Nominal grid power	5 kW
Nominal load voltage	48 V
Nominal battery voltage	150 V
Nominal supercapacitor voltage	48 V
Current control loop bandwidth	300 Hz
Main DC voltage control bandwidth	20 Hz
Auxiliary DC voltage control bandwidth	20 Hz
ESS HPF cutoff frequency (f_{cESS})	0.1 Hz
Battery LPF cutoff frequency (f_{cb})	0.5 Hz
Central control system frequency	100 Hz
Distributed control system frequency	10 kHz

The resultant control action of the closed loop power reference compensation is the extra ESS power reference ($P_{ESS}^{*\prime}$). As in the previous cases, a low-pass filter is used to determine the extra reference of the battery ($P_b^{*\prime}$) and the extra reference of the supercapacitor ($P_{sc}^{*\prime}$).

As in the case stated in Subsection III-B, a pure P controller and a PI controller will be implemented in order to perform the analysis of the closed loop power reference compensation. This way, it will be possible to observe the effects of applying an integral action in this compensation method.

IV. SIMULATION RESULTS

In order to validate the different compensation techniques, several simulations are carried out in MATLAB/Simulink with the parameters described in Table I: ideal case, open loop power reference compensation, auxiliary DC voltage control and closed loop power reference compensation.

A. Ideal case

First simulation (ideal case) has neither grid power restriction nor compensation. The results are shown in Fig. 7. Due to the limited bandwidth of the main DC voltage control, there are some small DC voltage deviations during the transients. Still, the system operation is nearly ideal. However, when the grid power exceeds the maximum power, the highlighted problem shown in Section II and Fig. 3 would arise. In the following discussion, limits to the grid power are set to ± 5 kW and the proposed compensation mechanisms are analyzed and compared.

B. Open loop power reference compensation

Second simulation case is performed by enabling the open loop power reference compensation presented in Subsection III-A. Results are shown in Fig. 8. As it can be seen, now the maximum grid power is accomplished. The DC voltage has a similar evolution than in the ideal case, except when saturation is produced. In that case, the DC-link voltage variations reflect the power mismatch problem. During saturation, the main DC voltage control loop generates the estimated power mismatch which is compensated by the ESS. When comparing

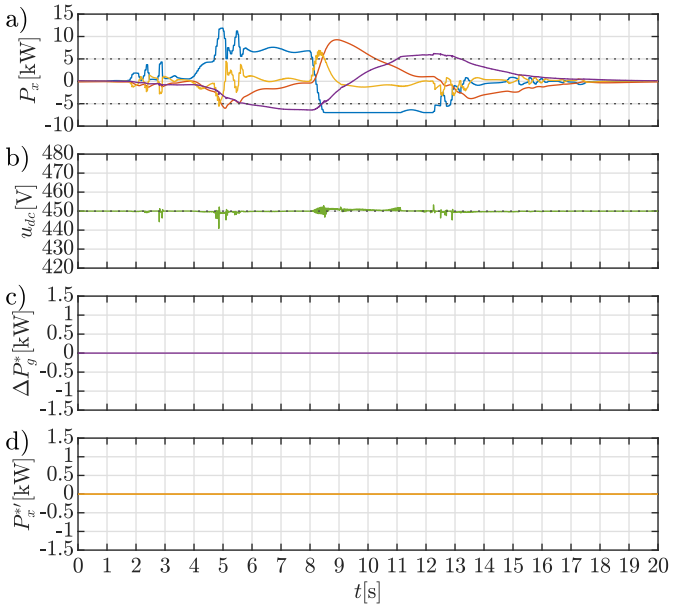

Fig. 7. Simulation results: Ideal case. a) Power consumption; b) DC-link voltage; c) Power mismatch given by grid controller; d) Extra power reference. Color legend: blue, load; red, battery; orange, supercapacitor; purple, grid; green, DC bus.

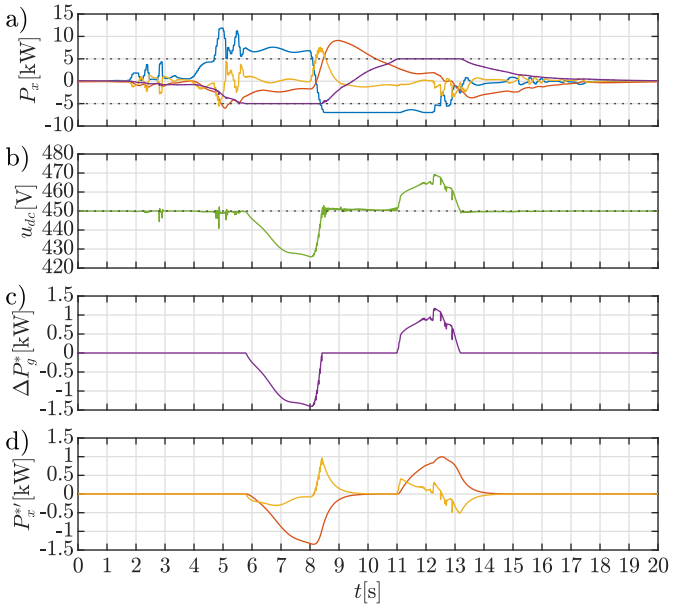

Fig. 8. Simulation results: Open loop power reference compensation. a) Power consumption; b) DC-link voltage; c) Power mismatch given by grid controller; d) Extra power reference. Color legend: blue, load; red, battery; orange, supercapacitor; purple, grid; green, DC bus.

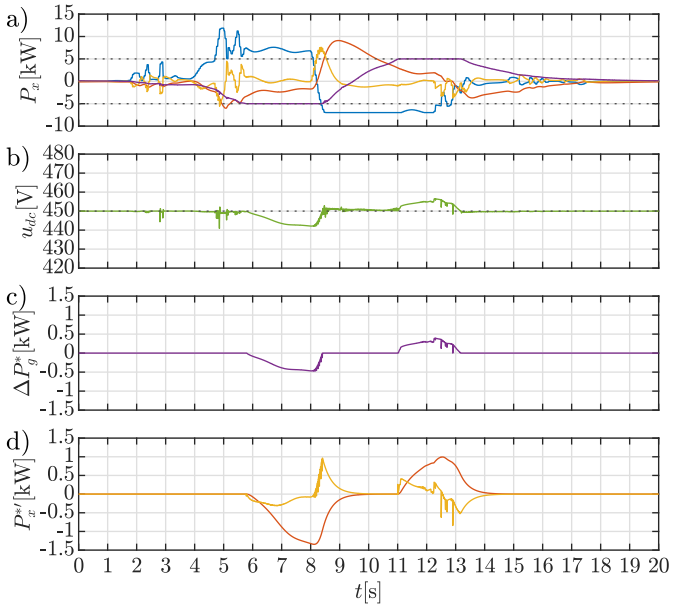

Fig. 9. Simulation results: Auxiliary DC voltage control with P controller. a) Power consumption; b) DC-link voltage; c) Power mismatch given by grid controller; d) Extra power reference. Color legend: blue, load; red, battery; orange, supercapacitor; purple, grid; green, DC bus.

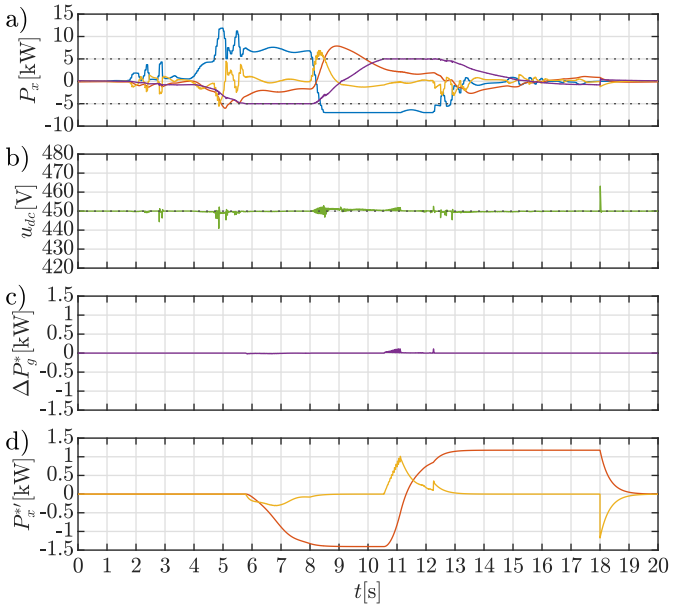

Fig. 10. Simulation results: Auxiliary DC voltage control with PI controller. a) Power consumption; b) DC-link voltage; c) Power mismatch given by grid controller; d) Extra power reference. Color legend: blue, load; red, battery; orange, supercapacitor; purple, grid; green, DC bus.

the DC-link voltage profile with the results shown in Fig, 3, the enhanced response is quite visible.

However, although the system continues operating within proper values, there is a noticeable variation of about ± 20 V in the DC-link voltage. This is produced because this compensation method does not take into account any feedback from the system (open loop), so any parameter deviation in the system will not be mitigated.

C. Auxiliary DC voltage control

Under this compensation method presented in Subsection III-B, two controllers are considered: P and PI structures.

Third simulation is performed by enabling the auxiliary DC voltage control with a proportional controller. Results are shown in Fig. 9. In this case, voltage variations during saturation are greatly improved compared to the open-loop compensation. This is because the analyzed compensation method is now using a closed control loop with the feedback signal of the DC-link voltage, which allows a better performance of the power sharing compensation.

Nevertheless, although the voltage variations are mitigated, the DC-link voltage is not completely corrected and some error is still present. Note that since there is not integral action, the proportional gain has to be tuned in order to fulfill the maximum DC-link voltage deviation requirements. In this case, it is 3 times the gain of the main DC voltage control.

Fourth simulation relies on the use of a PI controller for the auxiliary DC voltage control with a view to reduce the maximum error in the DC-link voltage during grid saturation events. Results are shown in Fig. 10. Now, it can be observed that the integral action is being applied whenever the auxiliary DC voltage control is enabled, so that the DC-link voltage error is completely canceled. The controller gains are equal to the ones of the main DC voltage control.

However, in this case, once the grid converter comes out of saturation, the auxiliary DC voltage control is disabled and hence the integral action is fixed to a constant value. This implies that the extra power references ($P_x^{*\prime}$) sent to both the battery and the supercapacitor may be stuck to a non-zero magnitude (Fig. 10), which is undesirable in the long run.

A possible solution is to reset the integral action whenever the auxiliary DC voltage control is disabled, but this causes a deterioration in the performance of the compensation method. The implemented solution also consists in resetting the integral action, but with a delay (some seconds) after disabling the auxiliary DC voltage control. In the simulated case, the reset of the integral action is produced at 18 s (5 s after coming out of saturation, which corresponds to 500 times the integral time) so that both extra power references evolve to zero at the expense of having a short DC-link variation during this time.

D. Closed loop power reference compensation

For the closed loop reference compensation proposed in Subsection III-C, also P and PI controllers are considered. The differences between the two approaches are here compared.

Fifth simulation is performed by enabling the closed loop power reference compensation with a proportional controller with a gain of 3. Results are shown in Fig. 11. As it can be seen, the results are similar to the ones obtained in Subsection IV-C with the P controller (Fig. 9) since the DC-link voltage variations are practically the same. Note that the proportional gain in both cases has the same multiplication fac-

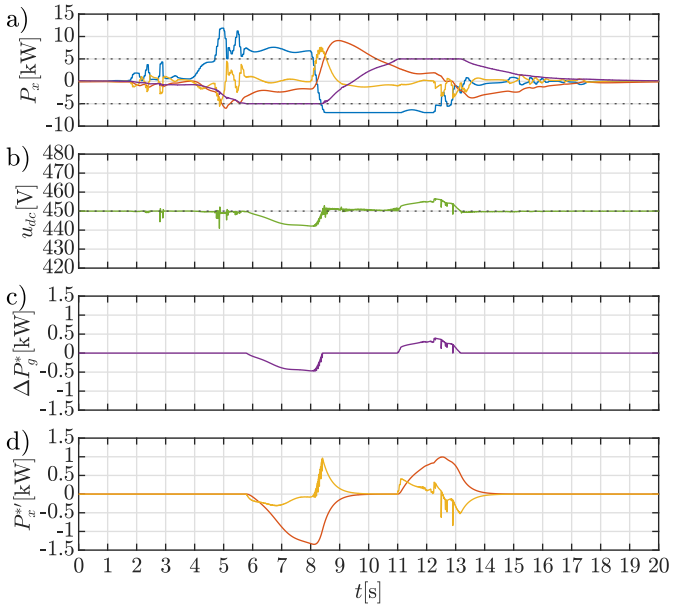

Fig. 11. Simulation results: Closed loop power reference compensation with P controller. a) Power consumption; b) DC-link voltage; c) Power mismatch given by grid controller; d) Extra power reference. Color legend: blue, load; red, battery; orange, supercapacitor; purple, grid; green, DC bus.

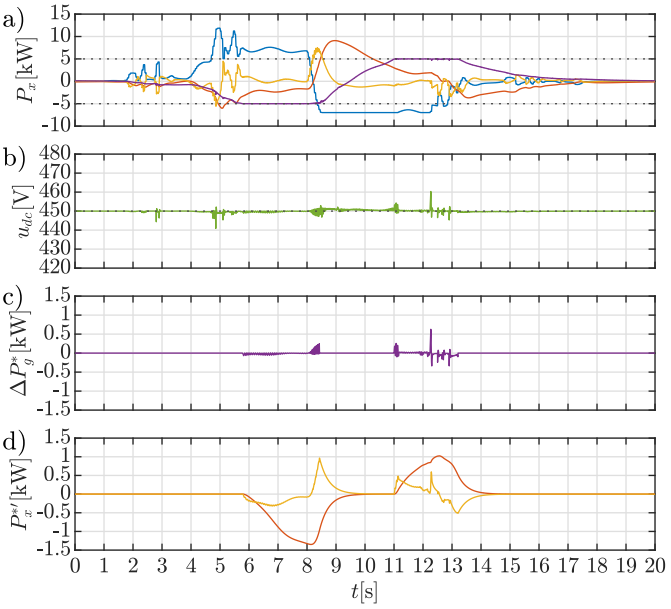

Fig. 12. Simulation results: Closed loop power reference compensation with PI controller. a) Power consumption; b) DC-link voltage; c) Power mismatch given by grid controller; d) Extra power reference. Color legend: blue, load; red, battery; orange, supercapacitor; purple, grid; green, DC bus.

tor (3), which could explain the similarities in their behavior. Nevertheless, if using a P controller, the closed loop power reference compensation would be chosen over the auxiliary DC voltage control since it is easier to implement.

That said, the proportional gain has to be tuned in order to fulfill the maximum DC-link voltage deviation requirements since no integral action is applied in this case.

Sixth simulation relies on the use of a PI controller for the closed loop power reference compensation with a view to reduce the maximum error in the DC-link voltage during grid saturation events. Results are shown in Fig. 12. At first glance, the results seems to be similar to the ones obtained in Subsection IV-C with the PI controller (Fig. 10) if the focus is on the variation of the DC-link voltage.

However, there are noticeable differences in the extra power reference ($P_x^{*\prime}$) commands. In contrast to the case of the auxiliary DC voltage control with PI controller, the control loop power reference compensation is operating continuously and hence the extra power references of both the battery and the supercapacitor automatically recover a zero value when the grid converter comes out of saturation. This way, the ESS is not forced to give extra power when the system is not in saturation for this compensation technique. This feature together with the fact that its implementation is easier makes the closed loop power reference compensation more suitable for this system than the auxiliary DC voltage control approach.

E. Summary

An overview of the key results (maximum grid power, integral of DC voltage error, maximum DC voltage error and DC voltage overshoot) for all the simulation cases is shown in Table II. As it can be seen, in all the cases with compensation, the maximum grid power is within the expected limits.

TABLE II
OVERVIEW FOR THE DIFFERENT SIMULATION CASES.

CASE	P_{grid}^{max} [kW]	$\int$|error| u_{dc}[V.s]	|error$_{\max}$| u_{dc}[V]	overshoot u_{dc}[%]
A) Ideal grid	6.4	5.3	9.1	1.2
B) OL pow ref comp	5.0	71.7	24.1	3.2
C1) Aux DC volt cont (P)	5.0	26.5	9.1	1.2
C2) Aux DC volt cont (PI)	5.0	5.5	13.2	1.8
D1) CL pow ref comp (P)	5.0	26.5	9.1	1.2
D2) CL pow ref comp (PI)	5.0	6.0	10.3	1.4

The open loop power reference compensation is the worst method for all the metrics, whereas the auxiliary DC voltage control and the closed loop power reference compensation achieve similar results. Overall, the implementations with PI controller obtain better results but their maximum voltage error (overshoot) is slightly worse when using a P controller.

Considering the integration of the auxiliary DC voltage control is more complex than the integration of the closed loop power reference, the last solution is the chosen one for the experimental validation.

V. EXPERIMENTAL RESULTS

In order to validate that the simulated results can be applied to a real system, the experimental setup shown in Fig. 13 is available for performing different tests.

The setup consists of two three-phase converters connected through the DC link (back-to-back configuration) and two inductor filters, which allow the interconnection of the different power units: AC grid, battery, supercapacitor and bidirectional load. The parameters of the experimental setup are the same

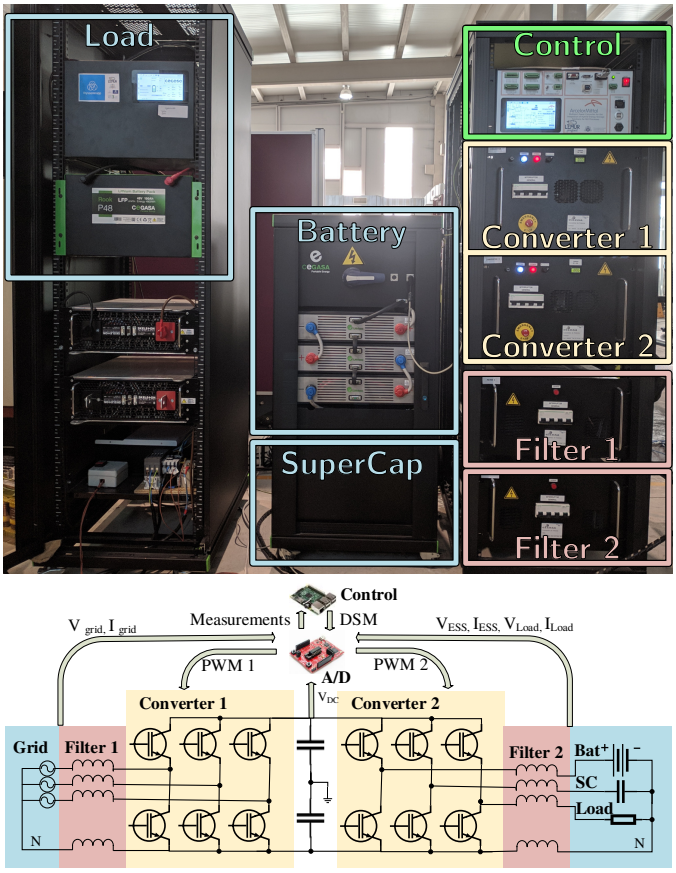

Fig. 13. Experimental setup: Front side and diagram.

as in the simulation (Table I) except the powers managed by the different power units, which are 10 times lower due to the current limitation of the converters.

The implementation of the control scheme is carried out by using two different control units: the microcontroller TMS320F28335 of Texas Instruments as the core of the distributed control system, and the single-board computed (SBC) Raspberry Pi as the core of the central control system.

Various experimental tests are carried out to demonstrate the suitability of the different compensation techniques and to address some problems that may appear during the real implementation: ideal grid, open loop power reference compensation and closed loop power reference compensation.

First experimental test verifies the results shown in Section II (Fig. 3), in which there is grid power restriction but no compensation. Results are shown in Fig. 14. As it can be seen, the DC-link voltage either drops to the rectifier level or rises to fault values when the grid power reaches the negative or positive limit.

Second experimental test is related to the simulation performed in Subsection IV-A, in which there is neither grid power restriction nor compensation. Results are shown in Fig. 15. As it can be seen, the DC-link voltage remains almost unchanged but the grid power exceeds the maximum power, so this case is not suitable for the requirements of the system.

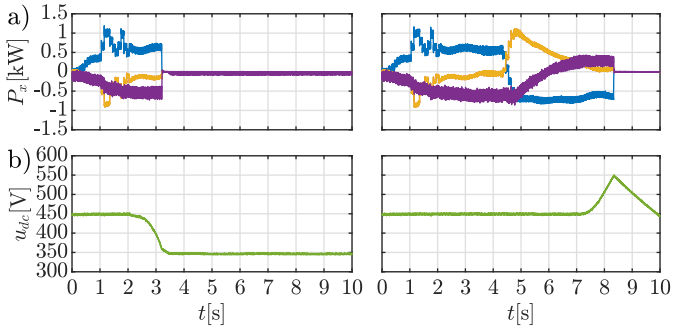

Fig. 14. Experimental results: Power sharing issues when the grid power is limited (left, negative; right, positive). a) Power consumption; b) DC-link voltage. Color legend: blue, load; orange, ESS; purple, grid; green, DC bus.

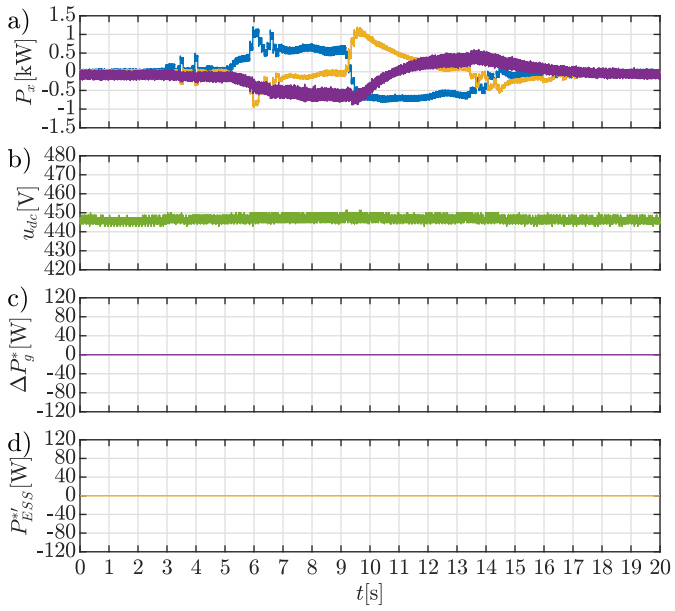

Fig. 15. Experimental results: Ideal case. a) Power consumption; b) DC-link voltage; c) Power mismatch; d) Extra power reference. Color legend: blue, load; orange, ESS; purple, grid; green, DC bus.

Third experimental test is related to the simulation performed in Subsection IV-B, in which the open loop power reference compensation is applied. Results are shown in Fig. 16. As it can be seen, the grid power is now limited to the maximum one. When the grid control reaches saturation, the DC-link voltage varies but its reference value is recovered by applying some extra power via the energy storage system.

Fourth experimental test is related to the simulation performed in Subsection IV-D, in which the closed loop power reference compensation with a P controller is applied. Results are shown in Fig. 17. As expected, this compensation method improves the performance of the open loop power reference compensation, with a noticeable reduction in the DC-link voltage variations.

VI. Conclusions

This paper has presented some compensation techniques of power sharing error, which can be applied to the DC

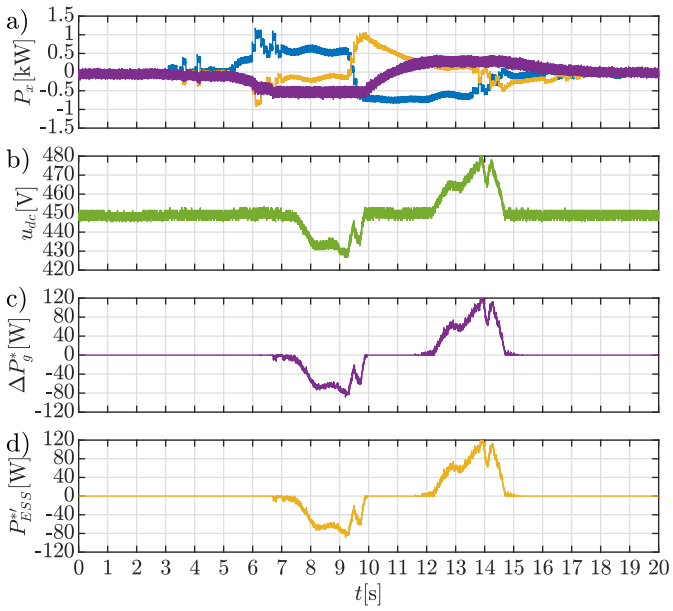

Fig. 16. Experimental results: Open loop power reference compensation. a) Power consumption; b) DC-link voltage; c) Power mismatch; d) Extra power reference. Color legend: blue, load; orange, ESS; purple, grid; green, DC bus.

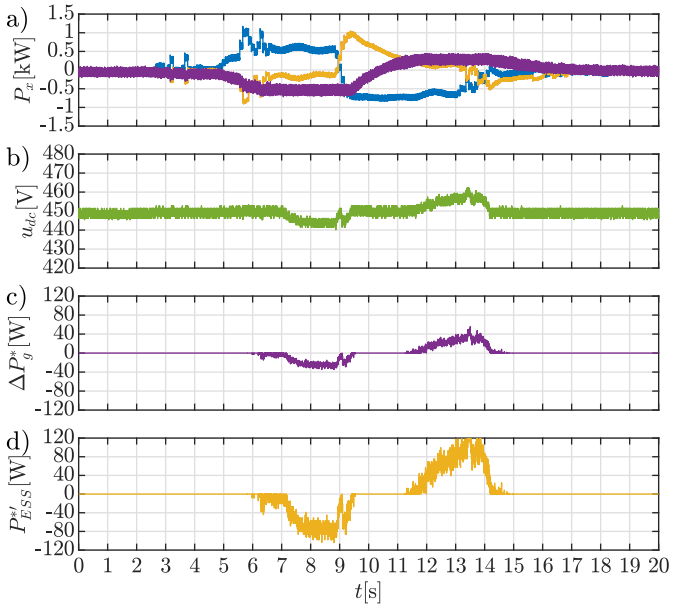

Fig. 17. Experimental results: Closed loop power reference compensation. a) Power consumption; b) DC-link voltage; c) Power mismatch; d) Extra power reference. Color legend: blue, load; orange, ESS; purple, grid; green, DC bus.

bus of hybrid microgrids. The proposed alternatives have been tested via simulations, obtaining proper results during saturation events and transient changes. Among the presented alternatives, the closed loop power reference compensation has the best tradeoff between implementation complexity and performance. Additionally, some experimental tests have been performed to verify that the system operates properly in a real situation.

REFERENCES

[1] T. S. Ustun, C. Ozansoy, and A. Zayegh, "Recent developments in microgrids and example cases around the world—a review," *Renewable and Sustainable Energy Reviews*, vol. 15, no. 8, pp. 4030 – 4041, 2011. [Online]. Available: http://www.sciencedirect.com/science/article/pii/S1364032111002735

[2] S. Vazquez, S. M. Lukic, E. Galvan, L. G. Franquelo, and J. M. Carrasco, "Energy storage systems for transport and grid applications," *IEEE Transactions on Industrial Electronics*, vol. 57, no. 12, pp. 3881–3895, Dec 2010.

[3] P. C. Loh, L. Zhang, and F. Gao, "Compact integrated energy systems for distributed generation," *IEEE Transactions on Industrial Electronics*, vol. 60, no. 4, pp. 1492–1502, April 2013.

[4] A. Mamen and U. Supatti, "A survey of hybrid energy storage systems applied for intermittent renewable energy systems," in *2017 14th International Conference on Electrical Engineering/Electronics, Computer, Telecommunications and Information Technology (ECTI-CON)*, June 2017, pp. 729–732.

[5] N. S. Jayalakshmi and D. N. Gaonkar, "Performance study of isolated hybrid power system with multiple generation and energy storage units," in *2011 International Conference on Power and Energy Systems*, Dec 2011, pp. 1–5.

[6] I. Peláez, S. Saheed, G. Villa, and P. García, "Optimization method for the integration of hybrid energy storage systems in industrial applications," in *2018 IEEE Energy Conversion Congress and Exposition (ECCE)*, Sep. 2018, pp. 6646–6653.

[7] Y. Cheng, V. M. Joeri, . Lataire, M. Lieb, E. Verhaeven, and R. Knorr, "Configuration and verification of the super capacitor based energy storage as peak power unit in hybrid electric vehicles," in *2007 European Conference on Power Electronics and Applications*, Sep. 2007, pp. 1–8.

[8] C. Renner and V. Turau, "State-of-charge assessment for supercap-powered sensor nodes: Keep it simple stupid!" in *2012 Ninth International Conference on Networked Sensing (INSS)*, June 2012, pp. 1–6.

[9] S. Saponara, A. Bove, F. Baronti, R. Roncella, R. Saletti, D. Dente, E. Leonardi, M. Marlia, and C. Taviani, "Thermal, electric and durability characterization of supercaps for energy back-up of automotive ecu," in *2013 IEEE International Symposium on Industrial Electronics*, May 2013, pp. 1–6.

[10] Y. Zhang and Z. Jiang, "Dynamic power sharing strategy for active hybrid energy storage systems," in *2009 IEEE Vehicle Power and Propulsion Conference*, Sep. 2009, pp. 558–563.

[11] G. T. Samson, T. M. Undeland, O. Ulleberg, and P. J. S. Vie, "Optimal load sharing strategy in a hybrid power system based on pv/fuel cell/battery/supercapacitor," in *2009 International Conference on Clean Electrical Power*, June 2009, pp. 141–146.

[12] R. Georgious, J. García, A. Navarro-Rodríguez, and P. García, "A study on the control design of nonisolated converter configurations for hybrid energy storage systems," *IEEE Transactions on Industry Applications*, vol. 54, no. 5, pp. 4660–4671, Sep. 2018.

[13] J. Garcia, R. Georgious, P. Garcia, and A. Navarro-Rodriguez, "Non-isolated high-gain three-port converter for hybrid storage systems," in *2016 IEEE Energy Conversion Congress and Exposition (ECCE)*, Sep. 2016, pp. 1–8.

[14] Y. Lu, J. Xu, Y. Zhao, P. Ye, and H. Li, "Optimal control of wind power hybrid energy storage system," in *2017 First International Conference on Electronics Instrumentation Information Systems (EIIS)*, June 2017, pp. 1–5.

[15] Y. Zhang and X. Xu, "Study on synergetic control for ultracapacitor/battery hybrid energy storage of wind/solar power system," in *2018 4th International Conference on Control, Automation and Robotics (ICCAR)*, April 2018, pp. 274–277.

[16] G. Villa, C. Gómez-Aleixandre, P. García, and J. García, "Distributed control alternatives of modular power converters for hybrid dc/ac microgrids," in *2018 IEEE Energy Conversion Congress and Exposition (ECCE)*, Sep. 2018, pp. 6379–6386.

[17] A. Navarro-Rodríguez, P. García, J. M. Cano, and M. Sumner, "Limits, stability and disturbance rejection analysis of voltage control loop strategies for grid forming converters in dc and ac microgrids with high penetration of constant power loads," in *2017 19th European Conference on Power Electronics and Applications (EPE'17 ECCE Europe)*, Sep. 2017, pp. P.1–P.10.